

RESEARCH ARTICLE

Open Access



Distance estimation technique from 360-degree images in built-in environments

Mojtaba Pourbakht^{1*}  and Yoshihiro Kametani¹

Abstract

The present study introduces a novel approach for quantifying distances within constructed environments. A mathematical model was developed for distance estimation in image processing using width and height estimation. In order to determine distance, the study employed the use of visual angle and sky view factor (SVF). Additionally, a camera with capabilities similar to the human eye was utilized to capture 360-degree photographs from a fixed position within a virtual reality corridor. The technique of Sky View Factor (SVF) is employed in indoor environments with ceilings by eliminating windows, doors, and roofs, thereby simulating a virtual sky. This enables the calculation of various parameters such as the image's area, area fraction, and aspect ratio through the utilization of image processing methods. Distance estimation can be predicted through the utilization of the sky view factor and visual angle, employing a linear regression analysis. The method of virtual sky view factor (VSVF) has potential applications in the fields of Engineering, robotics, and architecture for the estimation of indoor distances.

Keywords Fish-eye, Aspect ratio, Sky view factor, Field of view, Image processing, Visual angle

1 Introduction

The concepts of distance estimation and precise measurements are of paramount importance in various academic disciplines and research endeavors. The determination of distance plays a crucial role in aiding the operations of construction, industrial, and autonomous vehicles. In the study conducted by Kuenzel (2016), an examination is undertaken to explore the perception of space-distance in human beings. Norman (2005) asserts that there has been extensive research conducted on the estimation of accessibility. Thompson (2002) highlights the significance of estimating distance. According to Toye's (1986) findings, it was determined that the estimated distance and visual angle exhibit equivalence.

The determining factor for location is visibility. Toye's research findings indicate that humans possess the ability to discern between objects that are in close proximity and those that are at a distance. According to McCready (1985) and Norman (2005), it was posited that distance ratios possess a higher degree of precision compared to depth ratios. The findings of his study suggest that individuals possess the ability to accurately assess distance ratios in both indoor and outdoor environments. The authors of the study conducted by Norman et al. (2017) did not take into account the variable of visual perception ratio of vertical distances.

Geisler's study showcased the potential of utilizing two-dimensional retinal images to infer distance, three-dimensional shape, and distance distributions within natural systems. According to Burge Geisler (2013), individuals demonstrate a greater proficiency in estimating ratios as opposed to lengths. Furthermore, the process of estimating distances necessitates the utilization of vertical vision. In Viguier's (2001) study, a combination

*Correspondence:

Mojtaba Pourbakht
mahoroba2011@msn.com

¹ Department of Environmental and Urban Engineering, Kansai University, Osaka, Japan

of lasers, ultrasonic sensors, computer vision, and neural networks was employed to ascertain distance estimations. According to Tarro's (2012) research, there is an accurate estimation of the distance between built environments.

The utilization of image processing techniques in conjunction with 360-degree cameras enables the efficient examination and evaluation of various structures. During the early 2000s, fish-eye photography was widely observed. Aerial photography facilitates the acquisition of quantitative remote sensing data and the creation of three-dimensional computer models; Gurtner (2009), Greene (1986), Amad (2012), Wróyski et al. (2020), and Loddo (2021). These technologies are capable of quantifying the spatial separation between an image and an object. This is employed in the domains of transportation, urban planning, and architecture.

Regan and Spekreijse (1977) investigated the concepts of distance perception, visual angles, and spatial geometry. In a study conducted by Beier (2019), it was found that visual angles exhibit a higher level of effectiveness compared to physical angles. Gogel's (1998) findings contradicted prevailing perceptions regarding sight and space. Foley (1975) posits that human beings tend to inaccurately estimate distances. Enhancing the accuracy of distance estimation. Fukusima (1997) conducted a study wherein precise measurements of viewing angles were developed, without taking into consideration the potential presence of visual-spatial conflict. In his study, Foley (2004) employs a technique of ratio normalization to calibrate vision. The process of determining the distance between two points was conducted by Levin and Haber (1993a, 1993b) provides evidence that visual field offsets are greater than initially expected and are not influenced by the distance at which an object is viewed.

Researchers here employ the term "sky view factor" (SVF) in their investigations pertains to the extent of the visual field that is observable in front of the eye, given the presence of a stationary object positioned between the eye and the fovea. (Zakšek et al., 2011) The measurement of radiation using Steyn's (1980) fish-eye lens was based on the concept of the SVF. The computation of the sky view factor has been conducted through the utilization of solar radiation and diffusion ratios, as outlined in previous studies (Gurnsey et al., 2010; Oke, 1981). However, the potential correlation between the sky view factor and visual perception or field of vision has yet to be explored.

Current experiment employed the use of virtual sky view factor (VSVF) and field of view (FOV) as by Kastendeuch (2012). In their study, Sosa et al. (2014) utilized image processing techniques to ascertain the values of Vertical Spatial Frequency similar to VSVF and FOV in current experiment. (Table 1) According to the study

conducted by Kim et al. (2016), it was suggested that the generation of fisheye images could be achieved by utilizing 360-degree panoramas. Table 2 presents a comprehensive field of view (FOV) ratio.

To estimate image distance the study examines the visual angle that is concerned with determining the dimensions of an object depicted in a photograph and the utilization of the sky view factor. This paper aims to provide a comprehensive analysis of the theoretical framework, research methodology, obtained results, and potential implications for future research and practical applications.

2 Methods

2.1 A. Research summary

The present study involved the consideration and implementation of the following procedures;

- a. The researchers selected a virtual reality (VR) corridor as the experimental setting because it offers a reduced level of distraction (Gu et al., 2020a, 2020b).
- b. In this study, students utilized computer vision and virtual reality (VR) technologies to make estimations of width and height at specific points.
- c. 360-degree images were created in order to calculate distances, drawing inspiration from their application in robotic and autonomous vehicles (Iizuka, 1987).
- d. The process of calculating distances in this study incorporated stereo matching and structure-from-motion techniques for the 360-degree images.
- e. Multiple angle cameras were utilized, resembling the stereo image capture configuration described by Wan (2008).
- f. Scene distances were estimated through the process of image comparison.
- g. The utilization of optical flow was employed in order to estimate distances by analyzing image motion (Chukanov, 2021).
- h. Various novel techniques for estimating distance were investigated through the utilization of convolutional neural networks (CNNs) (Amirian, 2020).
- i. The consideration of distance estimation from 360-degree images was also discussed by Kiran (2020).
- j. In the study conducted by Touahni (2022), the researchers employed VR cameras and Structure from Motion (SfM) techniques to estimate distances within a virtual environment.
- k. Structure-from-Motion (SfM) photogrammetry was utilized as a methodology for the reconstruction of three-dimensional (3D) scenes.
- l. Both fish-eye and conventional images were utilized for Structure-from-Motion (SfM) techniques.
- m. Geometric equations were formulated in order to estimate distances.

Table 1 Simulation models establishment

	Zone 1			Zone 2			Zone 3			Zone 4			Zone 5			Zone 6			Zone 7		
Feature	VSVF	FOV	CV	VSVF	FOV	CV	VSVF	FOV	CV	VSVF	FOV	CV	VSVF	FOV	CV	VSVF	FOV	CV	VSVF	FOV	CV
1	●	●	●	●	●	●	●	●	●	●	●	●	●	●	●	●	●	●	●	●	●
2	●	●	●	●	●	●	●	●	●	●	●	●	●	●	●	●	●	●	●	●	●
3	●	●	●	●	●	●	●	●	●	●	●	●	●	●	●	●	●	●	●	●	●
4	●	●	●	●	●	●	●	●	●	●	●	●	●	●	●	●	●	●	●	●	●
5	●	●	●	●	●	●	●	●	●	●	●	●	●	●	●	●	●	●	●	●	●
6	●	●	●	●	●	●	●	●	●	●	●	●	●	●	●	●	●	●	●	●	●
7	●	●	●	●	●	●	●	●	●	●	●	●	●	●	●	●	●	●	●	●	●
8	●	●	●	●	●	●	●	●	●	●	●	●	●	●	●	●	●	●	●	●	●
9	●	●	●	●	●	●	●	●	●	●	●	●	●	●	●	●	●	●	●	●	●
10	●	●	●	●	●	●	●	●	●	●	●	●	●	●	●	●	●	●	●	●	●
11	●	●	●	●	●	●	●	●	●	●	●	●	●	●	●	●	●	●	●	●	●
12	●	●	●	●	●	●	●	●	●	●	●	●	●	●	●	●	●	●	●	●	●
13	●	●	●	●	●	●	●	●	●	●	●	●	●	●	●	●	●	●	●	●	●
14	●	●	●	●	●	●	●	●	●	●	●	●	●	●	●	●	●	●	●	●	●
15	●	●	●	●	●	●	●	●	●	●	●	●	●	●	●	●	●	●	●	●	●
16	●	●	●	●	●	●	●	●	●	●	●	●	●	●	●	●	●	●	●	●	●
17	●	●	●	●	●	●	●	●	●	●	●	●	●	●	●	●	●	●	●	●	●
18	●	●	●	●	●	●	●	●	●	●	●	●	●	●	●	●	●	●	●	●	●
19	●	●	●	●	●	●	●	●	●	●	●	●	●	●	●	●	●	●	●	●	●
20	●	●	●	●	●	●	●	●	●	●	●	●	●	●	●	●	●	●	●	●	●
21	●	●	●	●	●	●	●	●	●	●	●	●	●	●	●	●	●	●	●	●	●
22	●	●	●	●	●	●	●	●	●	●	●	●	●	●	●	●	●	●	●	●	●
23	●	●	●	●	●	●	●	●	●	●	●	●	●	●	●	●	●	●	●	●	●
24	●	●	●	●	●	●	●	●	●	●	●	●	●	●	●	●	●	●	●	●	●
25	●	●	●	●	●	●	●	●	●	●	●	●	●	●	●	●	●	●	●	●	●
26	●	●	●	●	●	●	●	●	●	●	●	●	●	●	●	●	●	●	●	●	●
27	●	●	●	●	●	●	●	●	●	●	●	●	●	●	●	●	●	●	●	●	●

- n. The study utilized the fish-eye triangulation technique—a method that involves the utilization of camera parameters and feature locations as a means to address the distortion caused by the lens (DING, 2021).
- o. Geometric equations were modified in order to achieve precise distance estimation.
- p. Fish-eye images, which possess the ability to capture a broad field of view, were employed.

Table 2 Image Processing via ED-IP (The content was generated by utilizing the area pixel count of the field of view (FOV) derived from the image processing techniques outlined in this study, along with regression analysis)

Fish-eye Shots	Z1		Z2		Z3		Z4		Z5		Z6		Z7	
	W	H	W	H	W	H	W	H	W	H	W	H	W	H
1	0.742468	3.195366	1.933704	2.600944	2.483378	2.170933	2.231134	2.581999	6.306037	4.422547	12.33194	5.432572	2.218833	8.245293
2	0.741192	3.205232	1.831769	2.463379	2.439686	2.132841	2.731729	2.184604	6.444076	4.519796	12.45382	5.48616	2.28591	8.49651
3	0.732753	3.179883	1.74994	2.33113	2.477423	2.165678	3.099239	2.476664	6.447365	4.521245	12.55604	5.531073	2.324946	8.642466
4	0.742709	3.224839	1.668468	2.242818	2.499482	2.184867	3.04821	2.435835	6.443899	4.518829	12.62454	5.561107	2.295006	8.532006
5	0.740451	3.215796	1.61847	2.17574	2.520366	2.203056	3.140335	2.509735	6.462203	4.531673	12.63563	5.565925	2.360207	8.775407
6	0.743379	3.228164	1.688496	2.269916	2.522349	2.2049	3.336007	2.665432	6.467421	4.535421	12.63415	5.565228	2.331662	8.616792
7	0.755206	3.282176	1.762859	2.369969	2.533171	2.214216	3.12454	2.497315	6.444417	4.519347	12.66918	5.580633	2.303021	8.561141
8	0.771037	3.352837	1.701694	2.287874	2.503056	2.187951	3.374003	2.695703	6.394811	4.484651	12.65512	5.574424	2.362744	8.785204
9	0.714135	3.09626	1.7976	2.41675	2.500895	2.012285	3.296577	2.634102	6.408047	4.493897	12.67049	5.581159	2.309835	8.586435
10	0.740176	3.210211			2.514847	2.198377	3.336944	2.666219	6.50232	4.559832	12.68483	5.587348	2.35819	8.76811
11	0.757055	3.2855			2.541897	2.221927	2.981816	2.383691	6.538643	4.583223	12.69429	5.591605	2.358146	8.768066
12	0.740639	3.178814			2.512761	2.196536	3.274288	2.616313	6.456117	4.527477	12.67331	5.582402	2.313995	8.603135
13	0.731658	3.157443			2.546355	2.225825	3.286709	2.636259	6.501466	4.559176	12.70688	5.597139	2.289648	8.511468
14	0.755069	3.286464			2.559129	2.236954	3.358372	2.683222	6.490346	4.551416	12.71667	5.601426	2.291527	8.518627
15	0.756197	3.292902			2.513147	2.196887	3.3576	2.6826	6.433473	4.511553	12.73068	5.607592	2.314206	8.602686
16	0.762523	3.324598			2.54782	2.22708	3.35304	2.679015	6.379189	4.473649	12.85537	5.662418		
17	0.759231	3.306261			2.494372	2.180527	3.290457	2.635757	6.339192	4.445622	12.95076	5.70443		
18	0.768127	3.345542			2.588454	2.262534	3.37587	2.697195			12.92835	5.694572		
19	0.779551	3.397676			2.551164	2.230074					12.74332	5.613164		
20	0.791557	3.450687			2.595441	2.268646					12.69712	5.592871		
21	0.740965	3.217785			2.526225	2.208355					12.69712	5.592871		
22	0.852426	3.693571			2.521945	2.2046					12.65375	5.573831		
23	0.777646	3.364206			2.444863	2.137353								
24	0.76874	3.33524			2.332728	2.039743								
25	0.767317	3.331752												
26	0.70727	3.06845												
27	0.718703	3.119708												

- q. Adjustments and calibration procedures were executed in order to optimize the accuracy of the 3D reconstruction.
- r. The utilization of sky view factor (SVF) calculations was employed for indoor spaces, taking into account obstructions (requiring calibration).
- s. The integration of field of view (FOV) and indoor sky view factor (SVF) was utilized to estimate distance, taking into account the pixel height.
- t. The aim of this study is to explore the development of a novel straight-gaze 360-degree field of view (FOV)
- u. The calculation of the field of view (FOV) is determined by the parameters of the camera sensor and lens.
- v. The technique of estimating distance by utilizing the field of view (FOV) and objects with known heights. (Table 2)
- w. The AR experiment utilized the camera features of SketchUp VR.

- x. The process of distance estimation incorporates the use of both panoramic and field of view (FOV) images.
- y. Fisheye panoramas were generated through the utilization of equal-distance projections. (Table 1)
- z. The process of feature matching was successfully accomplished through the utilization of SIFT/SURF algorithms, as described by Teke (2011).

Figure 1 depicts the primary methodology employed to render distance estimation perceptible. By conducting all of the evaluations, we were able to assess the inclinations of students to either overestimate or underestimate the dimensions of corridors as displayed in Fig. 2.

2.2 B. (FOV) and (SVF)

Fish-eye images encompass the entirety of the visual field perceivable by the human eye; however, they introduce

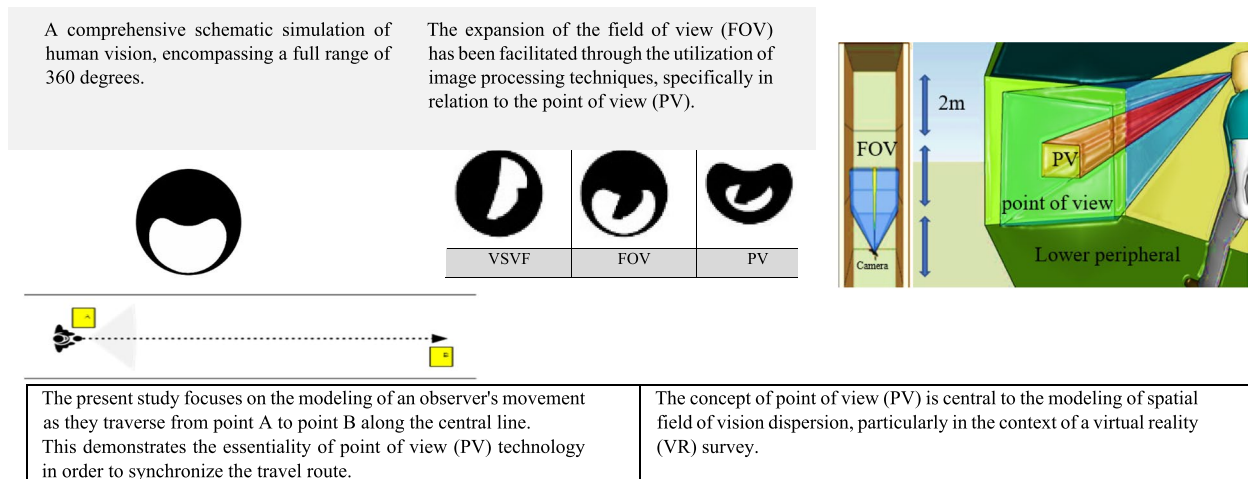
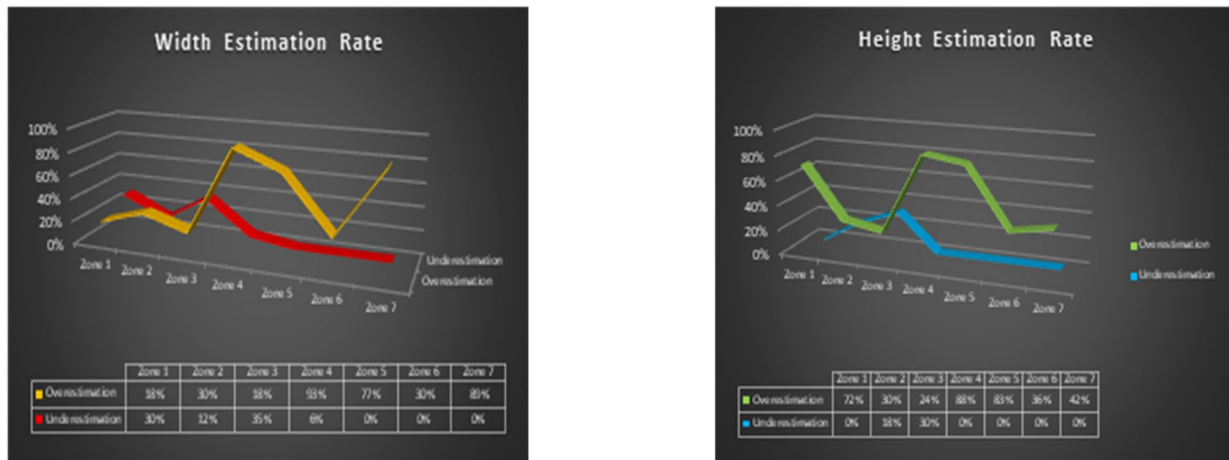


Fig. 1 Illustrates the schematic flow of a 360-degree simulation of human vision utilizing fish-eye lenses. The determination of the angle of view is contingent upon the visual capabilities of the human eye. (The designs were created using JW CAD and SketchUp software by the authors). The author(s) of this manuscript are responsible for creating all tables and figures, unless explicitly stated otherwise



It has been observed that students tend to overestimate or underestimate the dimensions of corridor width and height.

Fig. 2 Students overestimate and underestimate corridor width and height (based on the data provided by the attending students)

image distortions that result in a reduction in the precision of distance estimation. The estimation of image scale and distance is influenced by the field of view, which can be calculated as follows:

$$average\ viewpoint = height\ above\ ground / \tan(FOV/2) \quad (1)$$

The field of view (FOV) refers to the angular extent of the observable scene captured by a fish-eye lens. In order to establish a connection between the field of view and distance estimations, it is necessary to consider the impact of the field of view on the scale of the image. The

$$distance = (object\ height \times image\ sensor\ size) / (2 \times \tan(FOV/2) \times pixel\ height \times SVF). \quad (4)$$

relationship between the image scale and the field of view can be expressed by the following equation:

$$image\ scale = (sensor\ size \times distance) / (focal\ length \times object\ size). \quad (2)$$

By incorporating the concepts of field of view (FOV) and image scale, it is possible to adapt the equation in order to determine the distance between a camera and an object with a known size. The calculation of the SVF for indoor spaces can be determined using the subsequent formula:

$$SVF = A_{visible} / A_{ground} \quad (3)$$

The presence of walls, furniture, and other objects poses challenges to the measurement of indoor sky view factor (SVF). This phenomenon results in spatial

variation of the Spatial Variation Factor (SVF) within the room, thereby requiring the integration of images from multiple rooms to address this concern. The estimation of sky view factor (SVF) is influenced by the lighting conditions within a room. In the context of indoor structured visual field (SVF) analysis, the presence of intricate geometrical features and specific lighting conditions necessitates the need for calibration and processing. Conversely, in a virtual reality (VR) setting, such constraints are not required. The formula for calculating distance is given by the equation:

Our objective was to develop a panoramic field of view (FOV) of 360 degrees using either fish-eye or wide-angle lenses. The focal point of the image will be positioned at the center and surrounded by a circular shape. The concept of circumference pertains to the visual periphery. The formula to calculate the angular field of view (FOV) for an image is as follows:

$$\theta = 2 \times \arctan(d / (2 \times f)) \quad (5)$$

In this equation, θ represents the angular field of view, d corresponds to the diagonal measurement of the camera sensor, and f denotes the focal length of the lens. The equidistant projection is a cartographic technique that results in the flattening of circular fields of view.

$$x = r \times \sin(\theta) \text{ and } y = r \times \cos(\theta), \quad (6)$$

The equations for x and y are given by $x=r \times \sin(\theta)$ and $y=r \times \cos(\theta)$, where r represents the distance between the center of the field of view (FOV) image and a specific point on the image, and θ represents the angle associated with that point.

In order to identify the characteristics of the images, the SIFT/SURF algorithm was utilized to extract the features of each image. According to Yang (2009), Moisan's (2004). According to Ruan (2009), camera distance estimation involves determining the spatial positions of objects within a three-dimensional scene in order to ascertain their respective distances from the camera. Next step involves the calculation of the Area (in square pixels), Area Fraction (in percentage), and Aspect Ratio. The following equations are used to calculate the area fraction and aspect ratio of Area C.

$$\text{Area (px}^2\text{)} = \text{number of pixels in Area C} \tag{7}$$

$$\text{Area Fraction (\%)} = (\text{Area C} / \text{Total image area}) \times 100 \tag{8}$$

$$\text{Aspect Ratio} = \text{width of Area C} / \text{height of Area C} \tag{9}$$

$$\text{SVF} = (\text{Area of sky} / \text{Total image area}) \times 100 \tag{10}$$

The equation $ED=B(TD)+G(VA)$ can estimate distance. The regression coefficients for actual distance and visual angle are denoted as B and G, respectively. The estimation of the corridor's endpoint is derived from the fish-eye image obtained in Step 1 and the analysis of Area C.

The image processing technique represents the termination point of a corridor.

$$VA = 2 \times \arctan(D/2L) \tag{11}$$

The variable D represents the diameter of the fish-eye image, while the variable L represents the distance between the camera and the corridor.

$$ED \text{ estimates } TD. \tag{12}$$

equations presented below are employed to generate the data displayed in table [a]:

$$\text{Area (px}^2\text{)} = \text{Number of pixels in the object} \tag{13}$$

$$\text{Area Fraction (\%)} = (\text{Area of Object} / \text{Total Area of Image}) \times 100 \tag{14}$$

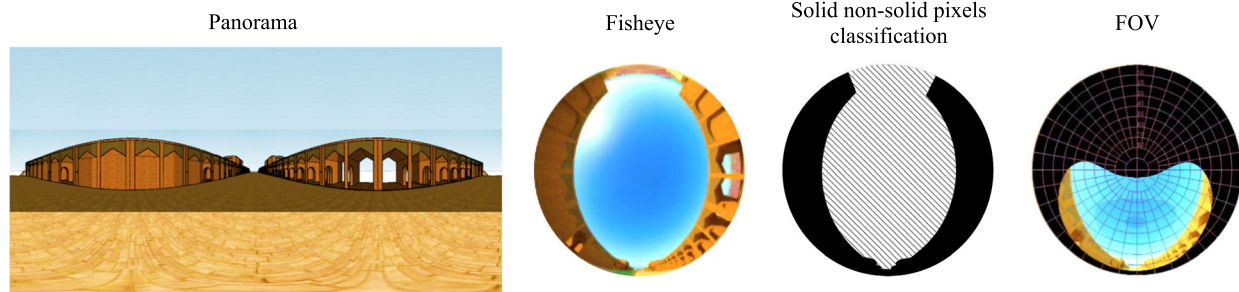
$$\text{Aspect Ratio} = \text{Major Axis Length} / \text{Minor Axis Length} \tag{15}$$

Figure 3 presents the aspect ratio associated with each study zone.

In order to address the analytical component of the project, a total of seven three-dimensional (3D) models were created. To capture comprehensive visual data, a virtual fish-eye camera with a 360-degree field of view was utilized to capture photographs from all possible angles. According to Luo et al. (2016), However, when the survey is conducted at two-meter intervals (as illustrated in Fig. 4), the field of view alters every six meters. Thus, a two-meter radius falls within this range, ensuring that all

a

Zone	VSVF	AR=FOV	PV	H	W
1	045704;	1.137015	1.520193	380	85
2	047333;	1.143156	1.516844	270	200
3	041208	1.155792	1.526104	240	275
4	048944	1.146672	1.523211	295	370
5	0.041412	1.158371	1.526947	490	700
6	041238	1.212733	1.541943	615	1400
7	0.043267	1.18464	1.535833	900	240



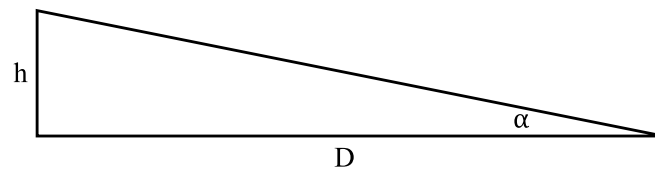
b

Fig. 3 a The conversion process from fisheye perspective to field of view (FOV) involves considering various parameters, including the virtual sky view factor (VSVF), aspect ratio (AR), point of view (PV), corridor height (H) measured in centimeters, and corridor width (W) also measured in centimeters. The transformation of a panorama to a viewing angle. (The table a content was generated by utilizing the area pixel count of the field of view (FOV) derived from the image processing techniques outlined in this study, along with regression analysis). Table 3 presents a comprehensive breakdown of the aspect ratio pertaining to each study zone

Feature	Area (px ²)	Area Fraction (%)	Filled Area (px ²)
1	31395	42.601262	45105
2	31062	42.212981	45123
3	31285	39.395313	45113
4	32140	43.792239	45078
5	31995	43.360709	45082
6	32156	41.163368	45047
7	33318	44.388489	45062
8	34694	48.667377	45063
9	31076	42.94816	46551
10	31869	46.624824	45103
11	33344	46.952799	45065
12	31077	46.50853	45103
13	30706	43.560789	45096
14	33365	46.868196	45053
15	33586	44.495966	45071
16	34212	43.795284	45054
17	33830	40.964351	45053
18	34671	47.601461	45073
19	35705	48.817337	45062
20	36837	51.136931	45046
21	32011	46.112071	45099
22	42009	55.585106	45045
23	34820	51.151722	45040
24	34349	48.367973	45059
25	34262	47.7027	45068
26	29327	44.752182	45323
27	30252	40.77089	45222

a

Based on the data presented in the graph below, it can be concluded that this assertion is indeed accurate. This suggests that in corridors exceeding a length of six meters, the visual attention is oriented towards the lower section rather than the upper section. According to the illustration presented in figure six, it can be observed that when the head and eyes are inclined downward by 10 degrees over extended



$Tan\alpha = h / D$
 $\alpha = 10\text{-degree}$
 $h = 110\text{cm}$
 $D = 624\text{cm}$

In instances where the length of a hallway exceeds six meters, it becomes impossible to observe parallel horizontal ceiling planes from any vantage point. Consequently, it is possible to eliminate

b

Fig. 4 a zone one, fraction, filled b minimum distance visible

possible points are captured. This is because the angle of view does not undergo significant changes over such distances. The study conducted by Newhall in 1956.

The ceilings in the hallways were removed as the typical adult refrains from rotating their head while ambulating. When an average adult, with a height of 170 cm, takes steps of 75 cm while walking straight ahead without rotating their head, the resulting angle of view to the ground is approximately 45 degrees. This calculation can be performed utilizing basic principles of trigonometry. If a right triangle is constructed, where one leg corresponds to half of the individual's height of 85 cm, and the other leg represents half of their stride length of 37.5 cm, the angle between the horizontal ground and the line connecting the person's eye to the center of their field of view (which is assumed to be directly in front of them) can be determined by evaluating the inverse tangent (arctan) of the ratio of these two lengths.

$$Tan(\theta) = adjacent/opposite = 85/37.5 \quad (16)$$

theta is equal to arctan (85/37.5) 63.4 degrees.

However, this particular perspective encompasses the complete range of visual perception from the earth's surface to an individual's eye level. Given our focus solely on the angle relative to the ground, it is necessary to subtract half of said angle, as the eye is positioned at an approximate midpoint between the ground and the individual's height.

$$\theta_{ground} = (63.4/2) 31.7 \text{ degrees.}$$

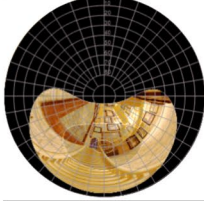
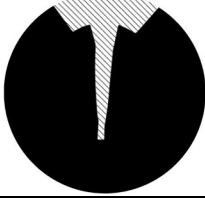
Given our focus on the complementary angle, which refers to the angle formed between the line of sight and the ground, we can derive this angle by subtracting it from 90 degrees.

$$\text{view angle} = 90 - 31.7 \approx 58.3 \text{ degrees}$$

Consequently, the angular separation between the eye of an individual and the central point of their visual field is estimated to be approximately 58.3 degrees. In order for the SVF concept to function effectively, it is imperative to exclude ceilings from consideration. To clarify, it can be stated that view frame adjustments primarily exhibit a linear characteristic. Given that the visual perspective is directed downwards (Loomis et al., 1996), individuals tend to concentrate their visual attention on vertical elements such as walls, rather than on the ceiling or windows, within such environments. According to the study conducted by Sakamoto et al. (2010).

Prior to its presentation, the circular fisheye image underwent a conversion process to an equirectangular projection. The horizontal and vertical field of vision (FOV) of the camera were subsequently determined based on the camera's specifications. The equation provided was utilized to ascertain the viewing angle of each

Table 4 FOV vs VSVF

Zone	Fisheye	Solid non-solid pixels classification	FOV	Rates
1				VSVF: 0.045704 H: 500 cm W: 85 cm FOV: 1.137015 PV: 1.520193
2				VSVF: 0.047333 H: 270 cm W: 200 cm FOV: 1.143156 PV: 1.516844
3				VSVF: 0.041208 H: 240 cm W: 275 cm FOV: 1.155792 PV: 1.526104
4				VSVF: 0.048944 H: 295 cm W: 370 cm FOV: 1.146672 PV: 1.523211
5				VSVF: 0.041412 H: 490 cm W: 700 cm FOV: 1.158371 PV: 1.526947
6				VSVF: 0.041238 H: 615 cm W: 1400 cm FOV: 1.212733 PV: 1.541943
7				VSVF: 0.043267 H: 900 cm W: 240 cm FOV: 1.18464 PV: 1.535833

G = the regression coefficient on visual angle (VA).

UE (B = 0.860, G = 0.175).

OE (B = 1.108, G = 0.164).

UE = Under Estimation.

OE = Overestimation.

IP = Image Processing

$$[IP]_W = (Orien \times W) + (AR \times Cent) \tag{22}$$

$$[IP]_H = (Orien \times H) + (AR \times Cent) \tag{23}$$

The pixel-formatted data is expected to be converted into SI units.

px to meter: $(px) \times (0.000264583333)$.

[IP]_W: Image processing width.

[IP]_H: Image processing height.

Orien = Orientation.

W: actual width.

AR: Aspect Ratio.

Cent: CentroidX.

To elucidate the interconnection among Eqs. 20, 21, 22 and 23, these equations delineate a methodology employing linear regression for the purpose of estimating distances by leveraging visual angle and sky view factor. The regression analysis yields coefficients that are subsequently employed in an equation incorporating true distance and visual angle, enabling the estimation of distances. Equations 22 and 23 seem to be integral components of a computational procedure in image processing, employed to preprocess the data in order to facilitate subsequent analysis. The precise functional representation of these relationships may differ depending on the dataset and the intended application, while the coefficients can aid in achieving a trade-off between overestimation and underestimation.

Table 5 presents the disparities between the estimated values and the actual distance ratios. Nevertheless, the standard error falls within an acceptable range for this particular test.

The calculation of standard deviation and error in this study is derived from the students' distance estimation data. These statistical measures quantify the extent to which the estimated distances deviate from the actual values. The calculations were performed using Microsoft Excel.

4 Discussion

The variable VSVF plays a crucial role in the methodology employed in this study. In order to improve the accuracy of the distance estimation ratio forecasting method, it would be beneficial to ascertain its value or aspect ratio

through the utilization of either Rayman's method or the approach outlined in the current literature. According to the study conducted by Matzarakis et al. (2009), The ratios of overestimation and underestimation are taken into account in order to ensure that the calculated final value falls within the range defined by these two extremes. (Levin 1993).

The deviation error and standard error are calculated based on the aspect ratio and estimated distance, as illustrated in Fig. 5. The table presents the specific measurements of corridor width and height for each research zone. The aforementioned ratios, particularly when juxtaposed with estimated values, suggest that the standard error is within the range of 1.8% to 6.9% of the true distance, which falls within an acceptable threshold. Based on the data presented in Table 5, it can be observed that both the deviation error and standard error exhibit relatively small magnitudes. This suggests that the estimation of the value is suitable and accurate.

Furthermore, it is imperative to conduct a meticulous assessment of the sky view factor, given its potential variability based on factors such as illumination, time of day, presence of furniture, and other obstructive elements. Despite its inherent limitations, this particular strategy possesses the potential for utility in a wide array of scenarios, with a particular emphasis on urban environments. The efficacy of this method necessitates further enhancement and evaluation to ascertain its suitability in various sectors, including virtual reality, robotics, and autonomous vehicles.

A method for estimating visual angles involves the utilization of the provided equation to calculate the visual angle of an object;

$$\text{Visual angle equals } 2 \arctan (\text{object size}/(2 * \text{viewing distance})). \tag{24}$$

The term "object size" refers to the physical dimensions of an object. The viewing distance refers to the spatial separation between an individual who is observing a particular object.

In order to employ the visual angle estimation technique for determining the distance of an object within an

Table 5 Based on height and width, estimate the distance deviation error

Zone	Width	Mean	Variance	Standard Deviation	Standard Error	Height	Mean	Variance	Standard Deviation	Standard Error
1	0.85	0.754014	0.004987	0.028104426	0.048082842	3.8	3.272089	0.14691	0.12534772	0.263955317
2	2	1.750334	0.035218	0.09547728	0.124833233	2.7	2.353391	0.067442	0.128800212	0.173304344
3	2.75	2.502962	0.032762	0.068493652	0.123518838	2.4	2.188006	0.024175	0.059637559	0.105996963
4	3.7	3.222504	0.12803	0.172363139	0.238747848	2.95	2.575058	0.079193	0.13730283	0.187470765
5	7	6.438825	0.159118	0.059390838	0.2805873	4.9	4.515374	0.074781	0.041541933	0.192313182
6	14	12.67933	0.880923	0.136249403	0.660334562	6.15	5.585099	0.161262	0.059837107	0.282450514
7	2.4	2.313592	0.004399	0.037783221	0.043204122	9	8.600884	0.089012	0.141665343	0.199558122

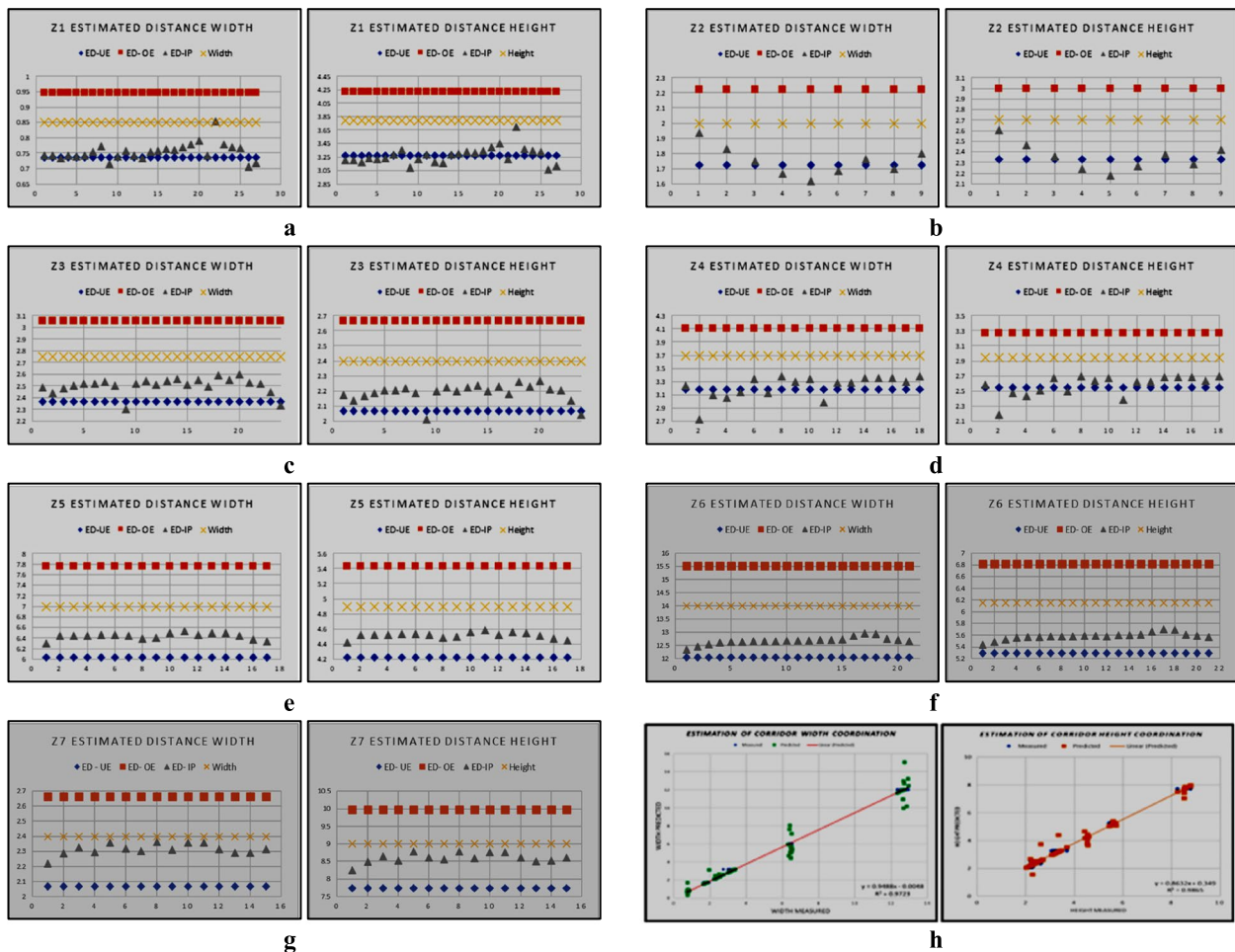


Fig. 5 Zone 1’s maximum, minimum, and ideal distances. Distances in zone 2. Zone 3 distances. Zone 4 distances. Zone 5 distances. zone 6 distances Relationships between distance and H-W correlations

image, it is imperative to possess prior knowledge regarding the object’s dimensions. In the absence of precise measurements, it is possible to estimate the dimensions of the object under scrutiny by employing a comparative analysis with a known reference object depicted in the image. After determining the size of the object, the aforementioned equation can be employed to compute the visual angle of the object. By establishing the correlation between visual angle and distance, it becomes possible to determine the precise distance of an object. The aforementioned correlation can be expressed in the following manner:

$$\text{Distance to object} = \text{object size} / (2 * \tan(\text{visual angle} / 2)) \quad (25)$$

The computation of the SVF can be achieved by utilizing the subsequent formula:

$$\text{SVF} = (A_{\text{sky}} / A_{\text{hemi}}) * 100\% \quad (26)$$

The term "sky" refers to the expanse of the visible atmosphere. The term "hemi" refers to the entirety of the hemispherical region that is perceptible from the vantage point of the observer.

Determine the Spatial Variation Factor (SVF) at the observer’s position by utilizing the equation provided above.

Utilize the provided equation to make an estimation of the distance to the object.

$$\text{Distance to object} = (\text{object size} / (2 * \tan(\text{visual angle} / 2))) / \text{SVF} \quad (27)$$

The aforementioned equation modifies the distance estimation by incorporating the influence of the sky view factor (SVF) on the visual angle. Factors such as atmospheric conditions, illumination, and the quality of the image may potentially influence the accuracy of the outcomes.

Figure 5g illustrates that the optimal projected distance ratio lies within the range of overestimation and the

actual proportion. A subsequent discovery was made. If the ratio between the average height and average width is below three, the subsequent equation can be employed to estimate the field of view (FOV) factor:

$$\sqrt[3]{(2e - \pi) \times |\arctan(H/3 + W/3 - (H \times W)/2)| \times HL} \quad (28)$$

Let e denote Euler's number, while H , W , and HL represent the average height, average width, and the limit of the horizon, respectively.

Table 4 illustrates the disparity between observed and projected ratios. This finding provides definitive evidence of a linear relationship between the variable and the prediction equation, establishing a clear connection between them. The coefficient of determination (R-square) in this particular case is 0.90, suggesting a strong correlation between the variables.

The authors generated these figures within the JW CAD environment.

5 Conclusion

The study incorporates the consideration of overestimation and underestimation ratios in order to ensure that the calculated distances ultimately fall within acceptable parameters. The accuracy of the method can be assessed by calculating deviation error and standard error, which are determined using aspect ratio and estimated distance. These measures indicate that the method's accuracy is within the range of 1.8% to 6.9% of the true distance, suggesting a satisfactory level of precision.

The study's findings indicate that the utilization of the Sky View Factor and visual angle estimation techniques shows potential for accurately determining distances in 360-degree photographs, despite the inherent difficulties associated with implementing these methods. The study underscores the necessity for further experimentation in order to ascertain the reliability of these findings.

Another outcome has emerged from the analysis, which involves the identification of a robust linear association between the variables and the predictive model. This is evidenced by a substantial coefficient of determination (R-square) value of 0.90. This finding indicates a strong correlation between the variables under investigation.

Nevertheless, this study is subject to certain limitations as a result of its execution within a controlled environment. Additional investigation is required to substantiate the results in practical situations, taking into account variables such as image quality and lighting conditions that could potentially impact the effectiveness of the visual angle estimation technique.

Abbreviations

AR	Aspect Ratio
VSVF	Virtual Sky View Factor
FOV	Field of View

CV	Central View
ED	Estimated Distance
TD	True Distance
B	The regression coefficient on true distance
VA	Visual Angle
G	The regression coefficient on visual angle
UE	Under Estimation
OE	Over Estimation
IP	Image Processing
IP_W	Image Processing Width
IP_H	Image Processing Height
Orien	Orientation
W	Actual Width
H	Actual Height
Cent	CentroidX

Acknowledgements

This declaration is "not applicable".

Authors' contributions

Both authors contributed to the project's achievement.

Funding

This declaration is "not applicable".

Availability of data and materials

Is contingent upon request.

Declarations

Consent for publication

Both authors agreed with the content and gave explicit consent to publish.

Competing interests

This declaration is "not applicable".

Received: 10 May 2023 Accepted: 10 September 2023

Published online: 13 October 2023

References

- Amad, P. (2012). From God's-eye to Camera-eye: Aerial Photography's Post-humanist and Neo-humanist Visions of the World. *History of Photography*, 36(1), 66–86. <https://doi.org/10.1080/03087298.2012.632567>
- Amirian, M., & Schwenker, F. (2020). Radial Basis Function Networks for Convolutional Neural Networks to Learn Similarity Distance Metric and Improve Interpretability. *IEEE Access*, 8, 123087–123097. <https://doi.org/10.1109/access.2020.3007337>
- Beier, S., & Oederkerk, C. A. (2019). Smaller visual angles show greater benefit of letter boldness than larger visual angles. *Acta Psychologica*, 199, 102904. <https://doi.org/10.1016/j.actpsy.2019.102904>
- Burge, J., & Geisler, W. (2013). Optimal retinal speed estimation in natural image movies. *Journal of Vision*, 13(9), 453–453. <https://doi.org/10.1167/13.9.453>
- Chukanov, S. N. (2021). The determination of distances between images of objects based on persistent spectra of eigenvalues of Laplace matrices. *Journal of Physics: Conference Series*, 1901(1), 012033. <https://doi.org/10.1088/1742-6596/1901/1/012033>
- Ding, J., Wang, Y., & Jiang, Y. (2021). Temporal dynamics of eye movements and attentional modulation in perceptual judgments of structure-from-motion (SFM). *Acta Psychologica Sinica*, 53(4), 337–348. <https://doi.org/10.3724/spj.1041.2021.00337>
- Foley, J. M. (1975). Error in visually directed manual pointing. *Perception and Psychophysics*, 17, 69–74.
- Foley, J. M., Ribeiro-Filho, N. P., & Da Silva, J. A. (2004). Visual perception of extent and the geometry of visual space. *Vision Research*, 44(2), 147–156. <https://doi.org/10.1016/j.visres.2003.09.004>
- Fukushima, S. S., Loomis, J. M., & Da Silva, J. A. (1997). Visual perception of egocentric distance as assessed by triangulation. *Journal of Experimental*

- Psychology: Human Perception and Performance*, 23(1), 86–100. <https://doi.org/10.1037/0096-1523.23.1.86>
- Glade, N. (2012). On the Nature and Shape of Tubulin Trails: Implications on Microtubule Self-Organization. *Acta Biotheoretica*, 60(1–2), 55–82. <https://doi.org/10.1007/s10441-012-9149-1>
- Gogel, W. C. (1998). An analysis of perceptions from changes in optical size. *Perception & Psychophysics*, 60(5), 805–820. <https://doi.org/10.3758/bf03206064>
- Greene, N. (1986). Environment Mapping and Other Applications of World Projections. *IEEE Computer Graphics and Applications*, 6(11), 21–29. <https://doi.org/10.1109/mcg.1986.276658>
- Gu, K., Fang, Y., Qian, Z., Sun, Z., & Wang, A. (2020a). Spatial planning for urban ventilation corridors by urban climatology. *Ecosystem Health and Sustainability*, 6(1), 1747946. <https://doi.org/10.1080/20964129.2020.1747946>
- Gu, K., Fang, Y., Qian, Z., Sun, Z., & Wang, A. (2020). Spatial planning for urban ventilation corridors by urban climatology. *Ecosystem Health and Sustainability*, 6(1). <https://doi.org/10.1080/20964129.2020.1747946>
- Gurnsey, R., Ouhanna, M., & Troje, N. (2010). Perception of biological motion across the visual field. *Journal of Vision*, 8(6), 901–901. <https://doi.org/10.1167/8.6.901>
- Gurtner, A., Greer, D., Glasscock, R., Mejias, L., Walker, R., & Boles, W. (2009). Investigation of Fish-Eye Lenses for Small-UAV Aerial Photography. *IEEE Transactions on Geoscience and Remote Sensing*, 47(3), 709–721. <https://doi.org/10.1109/tgrs.2008.2009763>
- Iizuka, M. (1987). Quantitative evaluation of similar images with quasi-gray levels. *Computer Vision, Graphics, and Image Processing*, 38(3), 342–360. [https://doi.org/10.1016/0734-189x\(87\)90118-6](https://doi.org/10.1016/0734-189x(87)90118-6)
- Kastendeuch, P. P. (2012). A method to estimate sky view factors from digital elevation models. *International Journal of Climatology*, 33(6), 1574–1578. <https://doi.org/10.1002/joc.3523>
- Kim, H., Jung, J., & Paik, J. (2016). Fisheye lens camera-based surveillance system for wide field of view monitoring. *Optik*, 127(14), 5636–5646. <https://doi.org/10.1016/j.jlleo.2016.03.069>
- Kiran, T. T. J. (2020). COMPUTER VISION ACCURACY ANALYSIS WITH DEEP LEARNING MODEL USING TENSORFLOW. *International Journal of Innovative Research in Computer Science & Technology*, 8(4). <https://doi.org/10.21276/ijrcst.2020.8.4.13>
- Kuenzel, R., Teizer, J., Mueller, M., & Blicke, A. (2016). SmartSite: Intelligent and autonomous environments, machinery, and processes to realize smart road construction projects. *Automation in Construction*, 71, 21–33. <https://doi.org/10.1016/j.autcon.2016.03.012>
- Levin, C. A., & Haber, R. N. (1993). Visual angle as a determinant of perceived interobject distance. *Perception & Psychophysics*, 54(2), 250–259. <https://doi.org/10.3758/bf03211761>
- Levin, C. A., & Haber, R. N. (1993b). Visual angle as a determinant of perceived interobject distance. *Perception & Psychophysics*, 54(2), 250–259. <https://doi.org/10.3758/bf03211761>
- Loddo, M. (2021). Integration of 360-Degree Photography and Virtual Reality into Museum Storage Facility Design and Education. *International Journal of Education (IJE)*, 9(4), 45–57. <https://doi.org/10.5121/ije.2021.9404>
- Loomis, J. M., Da Silva, J. A., Philbeck, J. W., & Fukusima, S. S. (1996). Visual Perception of Location and Distance. *Current Directions in Psychological Science*, 5(3), 72–77. <https://doi.org/10.1111/1467-8721.ep10772783>
- Luo, X., Chen, Y., Huang, Y., Tan, X., & Horimai, H. (2016). 360-degree realistic 3D image display and image processing from real objects. *Optical Review*, 23(6), 1010–1016. <https://doi.org/10.1007/s10043-016-0264-0>
- Matzarakis, A., Rutz, F., & Mayer, H. (2009). Modelling radiation fluxes in simple and complex environments: Basics of the RayMan model. *International Journal of Biometeorology*, 54(2), 131–139. <https://doi.org/10.1007/s00484-009-0261-0>
- McCready, D. (1985). On size, distance, and visual angle perception. *Perception & Psychophysics*, 37(4), 323–334. <https://doi.org/10.3758/bf03211355>
- Moisan, L., & Stival, B. (2004). A Probabilistic Criterion to Detect Rigid Point Matches Between Two Images and Estimate the Fundamental Matrix. *International Journal of Computer Vision*, 57(3), 201–218. <https://doi.org/10.1023/b:visi.0000013094.38752.54>
- Norman, J. F., Adkins, O. C., Dowell, C. J., Shain, L. M., Hoyng, S. C., & Kinnard, J. D. (2017). The visual perception of distance ratios outdoors. *Attention, Perception, & Psychophysics*, 79(4), 1195–1203. <https://doi.org/10.3758/s13414-017-1294-9>
- Norman, J. F., Crabtree, C. E., Clayton, A. M., & Norman, H. F. (2005). The Perception of Distances and Spatial Relationships in Natural Outdoor Environments. *Perception*, 34(11), 1315–1324. <https://doi.org/10.1068/p5304>
- Oke, T. R. (1981). Canyon geometry and the nocturnal urban heat island: Comparison of scale model and field observations. *Journal of Climatology*, 1(3), 237–254. <https://doi.org/10.1002/joc.3370010304>
- Regan, D., & Spekreijse, H. (1977). Auditory—Visual Interactions and the Correspondence between Perceived Auditory Space and Perceived Visual Space. *Perception*, 6(2), 133–138. <https://doi.org/10.1068/p060133>
- Ruan, L. F., Wang, G., & Sheng, H. Y. (2009). 3D position and attitude measurement based on marking-points recognition. *Journal of Computer Applications*, 28(11), 2856–2858. <https://doi.org/10.3724/sp.j.1087.2008.02856>
- Sakamoto, K., Okumura, M., Nomura, S., Hirotsu, T., Shiwaku, K., & Hirakawa, M. (2010). 360 Degrees All-Around View Displaying Using Viewing Angle Control Technique. *Ferroelectrics*, 394(1), 40–53. <https://doi.org/10.1080/00150191003678385>
- Sosa, J. M., Huber, D. E., Welk, B., & Fraser, H. L. (2014). Development and application of MIPARTM: A novel software package for two- and three-dimensional microstructural characterization. *Integrating Materials and Manufacturing Innovation*, 3(1), 123–140. <https://doi.org/10.1186/2193-9772-3-10>
- Steyn, D. (1980). The calculation of view factors from fisheye-lens photographs: Research note. *Atmosphere-Ocean*, 18(3), 254–258. <https://doi.org/10.1080/07055900.1980.9649091>
- Taibi, M., & Touahni, R. (2022). 3D Reconstruction Based on the SfM-MVS Photogrammetric Approach From Fundus Images. *SSRN Electronic Journal*. <https://doi.org/10.2139/ssrn.4090370>
- Takeshima, Y. (2021). Visual field differences in temporal synchrony processing for audio-visual stimuli. *PLoS ONE*, 16(12), e0261129. <https://doi.org/10.1371/journal.pone.0261129>
- Tarrío, P., Bernardos, A. M., & Casar, J. R. (2012). An Energy-Efficient Strategy for Accurate Distance Estimation in Wireless Sensor Networks. *Sensors*, 12(11), 15438–15466. <https://doi.org/10.3390/s121115438>
- Teke, M. (2011). High-resolution multispectral satellite image matching using scale invariant feature transform and speeded up robust features. *Journal of Applied Remote Sensing*, 5(1), 053553. <https://doi.org/10.1117/1.3643693>
- Thompson, P. (2002). Eyes Wide Apart: Overestimating Interpupillary Distance. *Perception*, 31(6), 651–656. <https://doi.org/10.1068/p3350>
- Toye, R. C. (1986). The effect of viewing position on the perceived layout of space. *Perception & Psychophysics*, 40(2), 85–92. <https://doi.org/10.3758/bf03208187>
- Viguier, A., Clément, G., & Trotter, Y. (2001). Distance Perception within near Visual Space. *Perception*, 30(1), 115–124. <https://doi.org/10.1068/p3119>
- Wan, D., & Zhou, J. (2008). Stereo vision using two PTZ cameras. *Computer Vision and Image Understanding*, 112(2), 184–194. <https://doi.org/10.1016/j.cviu.2008.02.005>
- Wróżyński, R., Pyszny, K., & Sojka, M. (2020). Quantitative Landscape Assessment Using LiDAR and Rendered 360° Panoramic Images. *Remote Sensing*, 12(3), 386. <https://doi.org/10.3390/rs12030386>
- Yang, Z. H., Chen, Y., Shao, Y. S., & Zhang, S. M. (2009). Scene matching algorithm for SAR images based on SIFT features. *Journal of Computer Applications*, 28(9), 2404–2406. <https://doi.org/10.3724/sp.j.1087.2008.02404>
- Zakšek, K., Oštir, K., & Kokalj, I. (2011). Sky-View Factor as a Relief Visualization Technique. *Remote Sensing*, 3(2), 398–415. <https://doi.org/10.3390/rs3020398>

Publisher's Note

Springer Nature remains neutral with regard to jurisdictional claims in published maps and institutional affiliations.